EUROFUSION WPHCD-PR(16) 16756

R McAdams et al.

Negative ion research at the Culham Centre for Fusion Energy (CCFE)

Preprint of Paper to be submitted for publication in
New Journal of Physics

This work has been carried out within the framework of the EUROfusion Consortium and has received funding from the Euratom research and training programme 2014-2018 under grant agreement No 633053. The views and opinions expressed herein do not necessarily reflect those of the European Commission.

Negative ion research at the Culham Centre for Fusion Energy (CCFE)

R McAdams[1], A J T Holmes[2], D B King[1], E Surrey[1], I Turner[1] and J Zacks[1]

[1]EURATOM/CCFE Association, Culham Science Centre, Abingdon, Oxfordshire OX14 3DB, UK
[2]Marcham Scientific, Hungerford, Berkshire RG17 0LH, UK

e-mail: roy.mcadams@ukaea.uk

Abstract. A summary of negative ion development work being presently undertaken at the Culham Centre for Fusion Energy (CCFE) is given. The Small Negative Ion Facility (SNIF) has an RF driven volume ion source with beam extraction at energies up to 30keV. The extracted beam of H^- ions has an associated co-extracted electron beam with an electron to ion ratio of <1 over the whole range of operating parameters. In order to understand this performance spectroscopic investigations have been undertaken using the Balmer series line to determine the electron temperature. In addition a 1D fluid model of an RF driven ion source is also under development. This model is based on a successful model for both arc discharge positive and negative ion sources. Additional system studies of neutral beam injection systems for future fusion machines beyond ITER are being carried out. This is required to understand the limits of various neutralisation and energy recovery systems in order to maximise overall electrical efficiency.

1. Introduction and historical perspective of negative ion development at CCFE

Work on the development of negative ion sources and accelerators began at Culham Laboratory, the home of the UK magnetic confinement fusion programme and the Joint European Torus (JET), in the early 1980s. With the construction of JET, which would use neutral beam injectors based on positive ion sources, underway at Culham, attention around the world began to turn to the requirements for future fusion machines. These would require higher injection energies for the neutral beams and to obtain good neutralisation efficiency negative ion beams must be used.

The initial work at Culham Laboratory focussed on negative ion sources and beams. Initially the application was for magnetically confined fusion machines but expanded to encompass applications in particle accelerators, defence and industry such as injectors of cyclotrons for medical isotope production. The first sources of H^- ions such as the Penning or magnetron sources relied on the use of caesium as a catalyst and were small in physical size, so making them of little use for large area beams such as neutral beam heating which requires many extraction apertures in parallel. At the start of the 1980's the development of H^- plasma sources that did not require caesium [1,2,3] began where the H^- ion was formed by a two step process where the first stage was the formation of highly vibrationally excited hydrogen molecules via fast electron impact and the second stage was a dissociative attachment collision with this molecule to form an H^- ion and atomic hydrogen. This process requires that the electron temperature is ~ 2eV. This low electron temperature also reduces the destruction of this ion by subsequent electron detachment collisions.

It was quickly realized that the earlier development of sources with a magnetic filter for proton fraction enhancement was the ideal method of realizing a large area practical source for beam heating in thermonuclear fusion type plasmas. The only major difference was the strength of the magnetic filter which is easily adjustable in any given source. The stronger filters reduce the electron temperature near the extraction apertures to slightly below 1eV which is ideal for H^- formation. Work was carried out to understand the role of the filter in controlling plasma transport in the ion source and its effect on electron temperature [4,5]. However the source plasma still contains a significant electron population and this must be handled by the accelerator attached to the source in a way that would permit multiple apertures if required [6,7,8,9].

A major program of experimentation followed, beginning with understanding how to form highly collimated H^- beams with current densities up to $220A/m^2$ and a low ion emittance [10,11] as this is essential in the development of neutral beam injectors. In parallel with this was understanding and suppressing the co-extracted electron current in the accelerator as these electrons represent a significant heat load in the accelerator, severe X-ray emission and reduce overall accelerator efficiency [12,13]. Another issue that affects future neutral beam injectors is the isotope effect between hydrogen and deuterium. This was examined for non-caesiated operation [14] where it was observed that deuterium negative ion beams have only approximately half of the current density of hydrogen sources.

This type of work ended at Culham Laboratory in the 1990s. Now with ITER under construction and design work underway for DEMO (which will come after ITER), development work on negative ion sources, accelerators and systems began again. This work has concentrated on modelling of ITER ion sources and components relating to both ITER and DEMO. Examples of this are understanding virtual cathode formation [15] due to the negative ion space charge at the caesiated wall of the ion source affecting the amount of negative ions which could be extracted, gas heating and target depletion due to plasma formation in the ITER neutraliser [16], the effect of plasma formation in the ITER beamline Residual Ion Dump [17] and space charge effects in the ITER ion beams [18].

The use of neutral beam heating and current drive requires a large amount of recirculating power in a fusion reactor for electricity generation which can affect the economic viability of such devices. Work at CCFE has investigated methods to improve the overall efficiency through increasing the neutralisation efficiency through the use of photo-detachment [19] and a beam driven plasma neutraliser [20] together with a novel concept which would allow energy recovery from the residual positive ions from the neutralisation process [21]. Overall systems studies of the injector systems for future fusion power generation have led to the understanding of how the design choices (and challenges) can lead to improvements in overall efficiency [21,22].

This paper will concentrate on this recent development work. In terms of negative ion source and accelerator physics a new negative ion facility using an RF ion sources has been built and this is described in Section 2. In section 3 the development of a 1D fluid model of RF driven ion sources is described and the results are compared to the measurements from SNIF. New system study results are then presented in Section 4.

2. The Small Negative Ion Facility

2.1 Ion source performance

A new H^- negative ion source and facility has recently been built at CCFE; namely the Small Negative Ion Facility (SNIF). SNIF was built to increase the number of smaller negative ion facilities within Europe. It operates at low extracted ion beam energy and current. This allows the facility to be used for developing and testing the physics and engineering of negative ion sources and beams in a very straightforward manner compared with much larger facilities. Changes to the facility and experiments can be turned around quickly giving a high degree of flexibility.

SNIF has been described previously by Zacks et al [23] and only a brief description is given here. Figure 1 shows a schematic of the ion source and accelerator. The ion source is cylindrical and is 30cm in diameter and 20cm deep. Multipole confinement magnets are arranged around the source body in rings in a chequerboard configuration. The ring of magnets closest to the plasma grid is arranged to give a dipole filter field across the source for negative ion production. The source back plate has a quartz window of 15cm diameter. A planar RF antenna is located at this window and the plasma is generated presently with a rf system at 13.56 MHz at powers up to 5kW. An automatic tuning network using two variable capacitors in an "L" network is used to match the output power from the RF generator to the load presented by the antenna and the plasma.

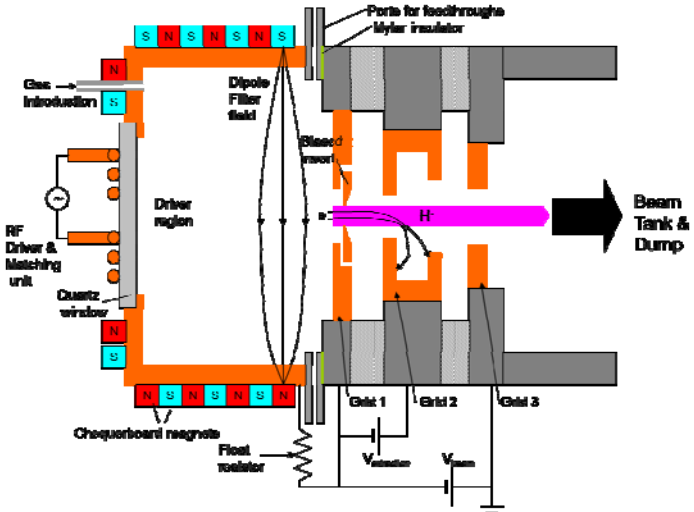

Figure 1 Schematic of the SNIF source and accelerator

A triode accelerator is used to extract the negative ions from a single aperture of 1.4 cm diameter (1.54 cm^2 area) at energies up to 30keV. The arrangement is very similar to those used for negative ion accelerators previously at CCFE [8,11]. The intermediate extraction electrode has a voltage of up to 6kV relative to the plasma electrode. The area around the extraction aperture is insulated from the main plasma electrode and can be biased relative to it with a voltage of up to 40V. This biased insert has a diameter of ~ 6cm.This arrangement allows control over the co-extracted electrons. Magnets are arranged in the plasma electrode in a quadrupole configuration where the field adds to the filter field in the source. Magnets are also located in the extraction electrode and in the earth electrode. These magnets along with those in the plasma grid produce fields which deflect co-extracted electrons into a recess in the extraction electrode, thus dumping them at low energy, and assist in re-steering the residual negative ion beam onto the central axis. The extracted beam drifts ~2m to a beam stop instrumented with 109 thermocouples to allow beam profile measurements. This diagnostic is also presently used to provide a beam current measurement at the beam stop. A 3D model of the beam stop has been used in the ANSYS system. The measured thermocouple time traces are modelled by inputting a beam profile on the

calorimeter front surface. The profile and input beam power are adjusted to fit the thermocouple traces hence giving a value for the beam current.

A McPherson 209 1.33m spectrometer is presently used to carry out spectroscopic measurements of the source plasma with a line of sight diagonally across the source through the extraction region at a distance of ~ 0.8 cm from the plasma grid. The optical fibre used for measuring the electron temperature by spectroscopy has a diameter of 200μm and is placed behind a 4.91mm diameter lens with a focal length of 15.15mm. This system has a full divergence angle of 0.0132rad.

In Figure 2 the beam currents derived from the ANSYS modelling are shown for a 25keV beam at two different bias voltages of the insert in the plasma grid and a gas flow rate to the source of 10sccm (~ 0.6Pa filling pressure in the ion source). The H^- current is lower at the higher bias voltage and reaches a maximum of 6mA (~39 Am^{-2}) at 3.5kW of RF power.

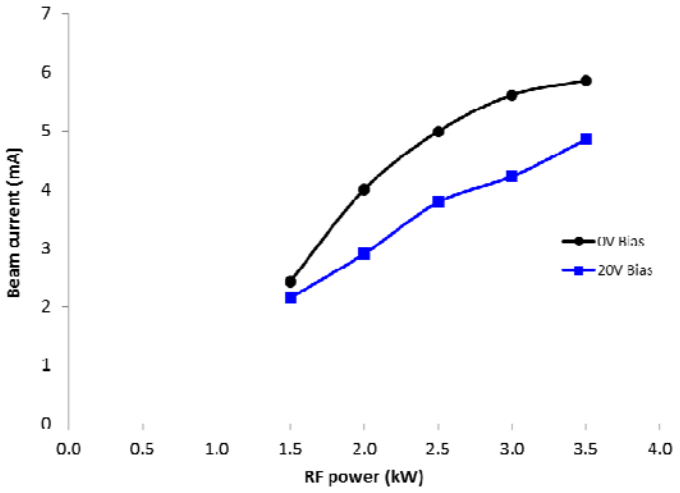

Figure 2 Beam currents at 25kV with 0V and 20V bias insert bias voltage and a gas flow rate of 10 sccm

The effect of insert bias voltage can also be clearly observed in the co-extracted electron current as measured by the extraction power supply as shown in Figure 3. In this figure the co-extracted electron current is plotted against insert bias voltage for a 25keV beam energy and a source gas flow of 10 sccm i.e. the same conditions as in Figure 2.

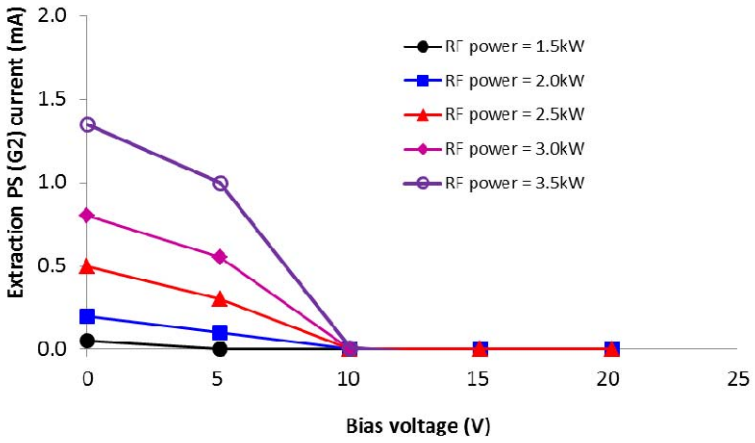

Figure 3 Co-extracted electron current at 25kV and a gas flow rate of 10 sccm

The co-extracted electrons fall rapidly as the bias voltage is increased to a point where at insert voltages higher than approximately 10V the current is zero. In all cases, comparing the data in Figure 3 with Figure 2, the ratio of co-extracted electron current to negative ion current much less than unity. This is a significant feature of operation of SNIF compared to operation of previous ion sources [14, 24].

2.2 Ion source plasma spectroscopy

The optical spectrometer has been used to carry out an initial spectroscopic investigation of the ion source plasma in order to attempt to understand the low extracted electron to negative ion current ratio. Measurements have been made of the intensities of the hydrogen Balmer series lines. By measuring the ratios of the line intensities the electron temperature of the plasma averaged along the line of sight can be deduced. In order to obtain the electron temperature a coronal model has been assumed. In the coronal model excitation of the hydrogen levels is assumed to be balanced by de-excitation by photon emission [25,26,27]. De-excitation by other particles e.g. metastables in the plasma is not accounted otherwise a collisional radiative model would be required.

The validity of the coronal model requires (i) that the plasma density is $< 10^{17}$ m^{-3} depending on the excited state and electron temperature, (ii) a Maxwellian temperature distribution for the electrons, (iii) the neutral pressure is < 500Pa, (iv) the electron temperature is much higher than the ion temperature and (v) the plasma is optically thin. These conditions are expected to be satisfied in the region between the magnetic filter field and the extraction plane where the plasma is viewed by the spectrometer. Thus under the coronal approximation the balance between electron excitation of a level j from the ground state and its decay by photon emission is

$$n_e N < \sigma v >_{0j} = N_j \sum_{k<j} A_{jk} \left(m^{-3} s^{-1}\right) \qquad (1)$$

where n_e is the electron density, N is the density of the ground state hydrogen atoms, $<\sigma v>_{0j}$ is the rate coefficient for electron impact excitation from the ground state to the level j, N_j is the density of the atoms in the excited state and the summation term gives the total transition probability of decay by transition from level j to levels k through the Einstein coefficients A_{jk}. Thus the total volumetric transition rate for a particular atomic transition involving level j → i, T_{ji}, is given by

$$T_{ji} = N_j A_{ji} = n_e N < \sigma v >_{0j} \frac{A_{ji}}{\sum_{k<j} A_{jk}} \left(photons\, m^{-3} s^{-1} \right) \qquad (2)$$

where the ratio of Einstein coefficients is the branching ratio of the particular transition. This total transition rate is proportional to the measured photon count rate for the transition where the constant of proportionality takes into account the transmission factor to the detector entrance, solid angle etc and the relative detection efficiency at the transition wavelength.

Hence, taking as an example the ratio of the Balmer alpha and beta lines, the ratio of the line intensities (as photon count rates) is given by

$$\frac{I(H_\alpha)}{I(H_\beta)} = \frac{< \sigma v >_{03}}{< \sigma v >_{04}} \frac{A_{32}}{\sum_{k<3} A_{3k}} \frac{\sum_{k<4} A_{4k}}{A_{42}} \frac{1}{R} \qquad (3)$$

where R is the relative detection efficiency of the two lines which can be obtained from a spectrometer calibration (in this case in terms of photon count rate). The Einstein coefficients are readily obtainable and the excitation rates are known as a function of electron temperature. The electron temperature can then be obtained from the line intensity ratio. Similar expressions can be simply written down for other line ratios.

It is instructive to compare the calculated line ratios in the coronal model given by equation 3 (for the case R=1) as shown in Figure 4. The electron impact excitation rates have been obtained from the HYDKIN collision data base [28]. For the H_β/H_γ line ratio, this is relatively insensitive to electron temperatures above 0.5-1.0eV. Furthermore, since the H_γ line has the smallest intensity of the three lines shown the ratio will be most prone to error. For the H_α/H_β line ratio the line ratio is insensitive to electron temperatures above ~ 1eV; these lines are the most intense. The H_α/H_γ line ratio is most sensitive to electron temperature except above a ~ 2eV but involves the low intensity H_γ line.

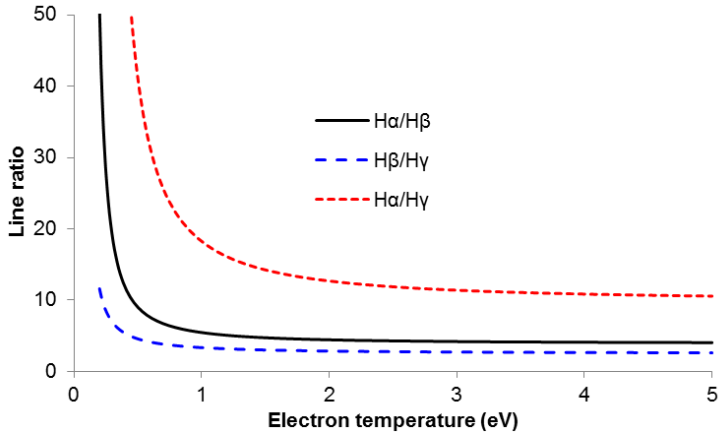

Figure 4 Calculated line ratios for the coronal model

These points are illustrated in Figure 5 where measurements of the electron temperature using the coronal model are shown for the three line ratios as the gas flow rate to the ion source is varied at an rf power of 2kW and 0V bias voltage. At high gas flow rates where the temperature is lower and the line ratios are most sensitive to the temperature, the three line ratios give good agreement. At low gas low rates where the temperature is higher the temperatures measured by the three line ratios are significantly different particularly the temperature derived from the H_β/H_χ ratio.

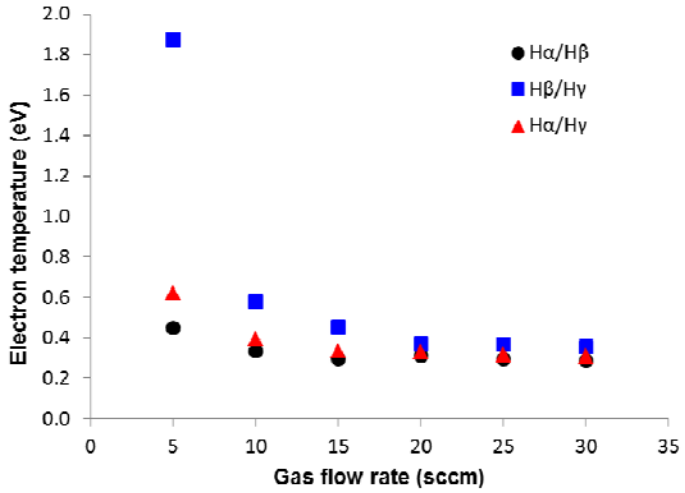

Figure 5 Measured electron temperatures at different source gas flow rates for an RF power of 2kW and 0V bias using the different line ratios

Measurements of the electron temperature from the coronal model using the lines ratio are used to compare the plasma parameters calculated from a 1D model of the source in Section 3.5 below.

3. 1D model of an RF driven ion source

A very successful model of arc discharge sources has been developed which is able to describe accurately the properties of both negative [29] and positive ion sources [30,31] using arc discharges. In these sources ionization takes place by primary electrons emitted by filaments according to an ionization rate which is determined by the local electron temperature and density. This ionization is controlled by the effects of the filter field which can modify both the density and local temperature. The plasma transport equations developed by Epperlein and Haines [32] allow the plasma density, temperature and local potential to be determined from the flow of electrons and electron energy through the filter region and there is an additional pair of equations for the flow of ions and ion energy. In the case of the ions, the energy flow equation is dropped because of the very strong coupling between the plasma ions and the background gas which can be used to obtain the gas temperature after assuming that the ions and gas have the same temperature.

In RF sources, ionization takes place throughout the source volume and there is no source of primary electrons. This arc discharge model has been modified to model RF sources. This RF source model makes extensive use of the model of Gudmundsson and Lieberman [33] and follows part of their approach but departs from them by using the transport equations. The gas temperature and division of the gas into atomic and molecular gas densities is almost identical to the theory of

DC sources [29]. That part of the model is incorporated here to obtain the density of negative ions and positive species fractions

3.1 The antenna region

In RF sources, it is the thermal electron population that causes ionization, and is characterised by the energy cost (in eV) per ionization event; ε_H for atomic hydrogen and ε_{H2} for molecular hydrogen. In the case of hydrogen this has been calculated by Hjartarsen et al [34] and is shown in Figure 6 for both atomic and molecular collisions. In the numerical code presented here, this energy cost has to be expressed as an empirical formula which is a function of the electron temperature near the antenna at the rear of the source, denoted by T_a.

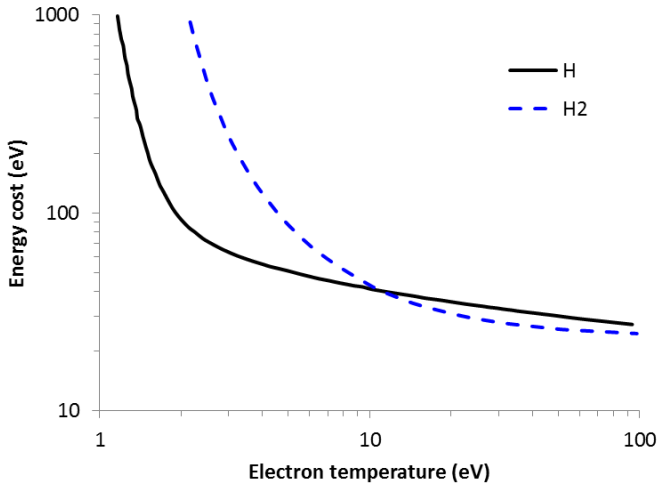

Figure 6 The energy cost to create a single electron-ion pair in atomic or molecular hydrogen

Gudmundsson and Lieberman [32] argue that there is an additional energy cost arising from the need for the electrons and ions to escape the plasma. The electrons remove $2eT_a$ each and the ions remove the plasma potential energy, $e\phi_a$ plus an additional $eT_a/2$ in the pre-sheath, where ϕ_a is the plasma potential at the antenna as with T_a. The base of the source is at another potential, $-\phi_G$, relative to the local plasma and there may be a power supply of voltage, V_G, to further bias this electrode relative to the plasma. In the experimental data presented in section 4.2.5, this power supply is absent so the plasma electrode floats. However the actual knife edge of the extraction aperture is biased positive to the plasma grid in order to suppress electrons, but this aspect of the experiment is not included in the model at present but may be incorporated later following the work of Haas and Holmes [12]. Thus all surfaces are negative, so the quartz plate and sidewalls are at $-\phi_a$ volts relative to the plasma and ϕ_a and ϕ_G are positive numbers. However the plasma source has a distribution of temperatures, being highest near the antenna and lower elsewhere. This is accounted for by introducing the parameter ψ which increases the average energy cost for a single electron-ion pair when such pairs are created far from the antenna where the plasma is cooler. Typically ψ has a value of 0.7 ± 0.05.

3.2 The main discharge

We can create a power balance using the RF power, P_{rf}, supplemented by the bias power, $I_G V_G$ and equating it to the power removed by escaping ions and electrons and power removed by gas cooling on the walls, P_{gas}. For a fraction, F, of atomic gas the power balance yields the total ion current, I_{ion}:

$$I_G V_G + P_{rf} - P_{gas} = \left[F \times (\varepsilon_H + 2.5T_a + \phi_a) + (1-F) \times (\varepsilon_{H2} + 2.5T_a + \phi_a)\right] \times \frac{I_{ion}}{\psi} \qquad (4)$$

It is assumed that the plasma is uniform in the radial direction as the magnetic cusp confinement on the sidewalls prevents the plasma adopting a radial Bessel shaped distribution. The total ionic current, I_{ion}, flows to three surfaces; the quartz plate, I_a, the sidewalls, I_w, and the grid, $f_i I_{ion}$. There is also a recombination current, I_{rec}. Summing the ion fluxes:

$$I_{ion} = I_a + I_w + f_i I_{ion} + I_{rec} \qquad (5)$$

The factor f_i represents the fraction of the total ionization current, I_{ion}, going to the plasma grid and I_{rec} is the recombination current.

The total ion current, I_{ion}, must be equal to the total ionization so:

$$I_{ion} = en_a \delta L \, A_G \left(N_H S_H(T_a) + N_{H2} S_{H2}(T_a)\right) \qquad (6)$$

where δ is the fractional depth of the source at which the ionization remains at the same level as at the antenna, and L is the total length of the source, making the effective depth equal to δL, S_H and S_{H2} are the ionization rates for atomic and molecular hydrogen with number densities N_H and N_{H2} respectively, and A_G is the plasma grid area. S_H and S_{H2} remain at the level set in the driver region at a temperature and density T_a, n_a at the antenna. An initial value for δ is 0.5 but this is improved in later numerical cycles in the model.

3.3 Gas density and temperature and plasma transport

This part of the model follows the approach initially developed by Chan [35] and includes the same processes and the solution method is virtually identical to the DC transport model [35,36,37]. The gas density and temperature depend on the interaction between the three positive ion species and electrons with the gas with the only major difference being the fact that thermal electron rates must be used rather than the fast primary electron rates used in references [29,30,31]. The division into atomic or molecular gas depends on recombination at the wall and this is assumed to be the same as in the DC model. The same methodology as that of Chan [35] is used to create the positive ion species (H^+, H_2^+ and H_3^+) fluxes and the positive ionic transport coefficients depend of the relative fraction of each species.

The gas temperature is very important as it sets the gas density in conjunction with a known gas flow rate and cold gas filling pressure. As in references [29,30,31], it is assumed that the main source of energy is the electron population which heats the ion population by Coulomb energy transfer. These ions are then assumed to have the same temperature as the gas atoms or molecules because of the very high collisionality, and the latter then accommodate on the source walls. In this way the electron energy transfer and wall accommodation set the ion and gas temperatures. The model can only converge slowly, so these processes will be treated as perturbations that are initially very small, and the rates for the various processes are described by empirical equations similar to those shown above to allow the numerical model to converge smoothly.

Once a preliminary estimate of the atomic and molecular fractions and gas densities is known, the plasma transport equations can then be solved, since the collision frequencies that control transport depend on both the gas density and local plasma density, which are known by this stage. As the ion temperature is the same as the gas temperature, the ion energy flux equation is dropped, leaving just three equations with three major control gradients; the plasma density gradient, the plasma electron temperature gradient and finally the potential gradient or plasma field

A similar approach is developed for the negative ion density based on the volume production of negative ions via highly vibrationally excited molecules. The negative ions are formed by dissociative attachment collisions between vibrationally excited hydrogen molecules and cold electrons whose temperature is less than 2eV [1]. Above this temperature, the rate coefficient decreases rapidly and at the same time the electron detachment rate rises significantly, sharply reducing negative ion formation. The vibrationally excited molecules are formed by collisions between electrons and molecules in the lowest vibrational state ($\upsilon = 0$). These excited molecules are destroyed by wall collisions and electronic excitation or ionization thus allowing a rate balance to be established:

$$N_{(\nu\geq 8)} n_a \frac{R_{in}}{T_a} + \frac{N_{(\nu\geq 8)}}{t_H} = N_{H2} n_a S_P \tag{7}$$

The term, t_H, is the transit time of an atom across the source, S_P is the production rate of these vibrationally excited molecules and R_{in}/T_a is the loss rate for these molecules via inelastic collisions [36]

Only vibrational levels in excess of 8 are included as the lower levels have a dissociative attachment rate that is roughly a factor of 5 lower for each level below 8. This is reflected in the value of S_P, the rate coefficient for production from levels with $\upsilon \geq 8$. A similar rate balance equation can be written for the negative ions. The production rate, S_{DA}, by dissociative attachment with vibrationally excited molecules above $\upsilon = 8$ is balanced by losses by ion-ion recombination with a rate, S_{II}, electron detachment with a rate, S_{EV}, and also loss by atomic gas collisions with a rate, S_H. Wall losses are neglected as it is assumed that there is a dense plasma and hence small mean free path. This gives a balance equation:

$$N_{(\nu\geq 8)} n_e S_{DA} = n_- n_e S_{EV} + n_- N_H S_H + n_- n_+ S_{II} \tag{8}$$

Replacing the negative ion density, n_- , by the fractional negative ion density, $q = n_-/n_+$, and assuming local plasma neutrality, gives a quadratic equation in q:

$$0 = -n_e S_{EV} q^2 + q\left(n_e (S_{EV} + S_{II}) + N_H S_H + N_{(\nu\geq 8)} S_{DA}\right) - N_{(\nu\geq 8)} S_{DA} \tag{9}$$

The transport coefficients for negative particles (electrons or ions) depends on this parameter, q so if $q = 1$, the plasma is a negative ion/positive ion plasma and if $q = 0$, it is a normal plasma. The former is insensitive to magnetic fields while the latter depends strongly on these fields, and at the same time the filter field induces strong cooling of the electron temperature. This can only be solved by slow numerical convergence with strong under-relaxation.

3.4 The Extraction Region

The plasma grid creates some boundary conditions where the electrode current, I_G, is:

$$I_G = I_{ion} f_i \left(f_e - 1 \right) \tag{10}$$

At present all the experimental data is with an I_G value of zero (floating) so f_e (the electron fraction to the grid) is unity in the code. The code loops until the ion current and negative charge current to this grid are equal. The code is quite "stiff" as only very small changes near the antenna lead to large changes near the grid. Therefore many cycles are needed as well as very slow stepping through the magnetic filter, particularly if the magnetic field is high. A typical solution brings the two fluxes to equality within ~1% in about 1000 major cycles and about ~1000 steps through the magnetic filter.

3.5 Comparison of results from SNIF

The SNIF source has been modelled using the RF ion source model described in the previous section and the output from the model has been compared with existing SNIF data. An important aspect of this was to apply the correct magnetic filter field to the model. From previous field measurements inside the source, it has been found that the field sharply increases as the plasma grid is approached, and this is due to a residual field from the accelerator magnets. Figure 7 shows the measured SNIF source field with an appropriate fit which was incorporated into the model in order to best represent the SNIF field.

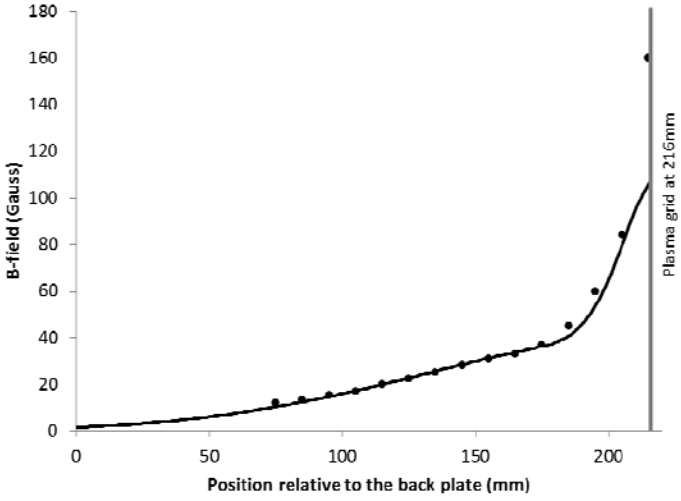

Figure 7 SNIF magnetic field present in the source measured along the central beam axis with a double Gaussian fit

The model is able to calculate various source parameters along the length of the source from the transport equations by Epperlein and Haines [32], and at different RF powers and source gas pressures. From the transport equations we are able to calculate the plasma density, temperature and potential as the model steps through the source; these results for a source gas pressure of 0.6Pa (which is equivalent to a gas flow of 10sccm on SNIF) and various RF power settings are shown in the Figures 8, 9 and 10:

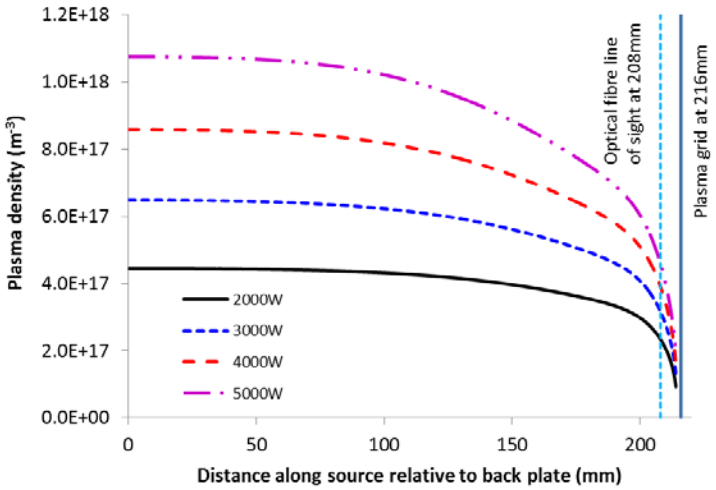

Figure 8 Model output of the SNIF plasma density along the central source axis at 10sccm gas flow and RF power 2000, 3000, 4000 and 5000W

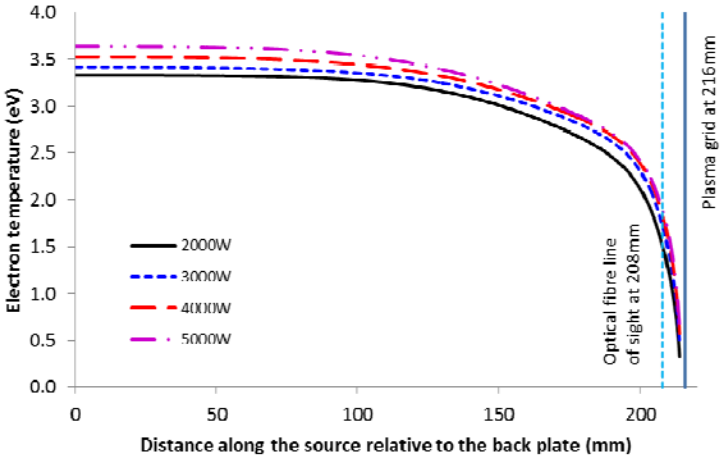

Figure 9 Model output of the SNIF plasma temperature along the central source axis at 10sccm gas flow and RF power 2000, 3000, 4000 and 5000W. Also shown is the line of sight of the optical fibre where spectroscopy measurements were taken in order to determine T_e

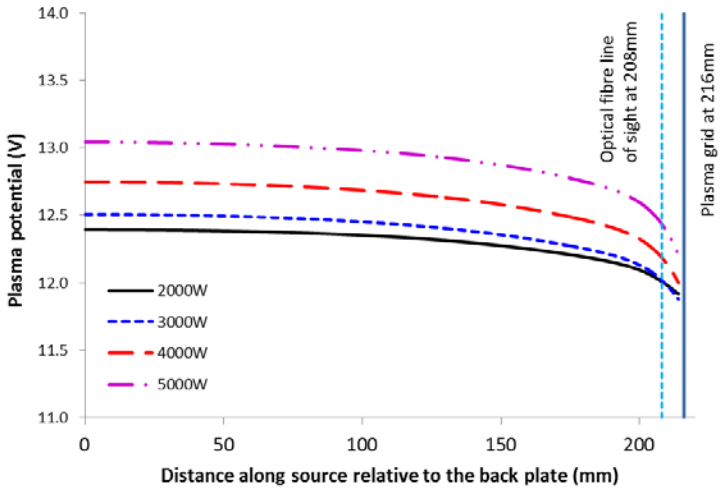

Figure 10 Model output of the SNIF plasma potential along the central source axis at 10sccm gas flow and RF power 2000, 3000, 4000 and 5000W

It can be deduced from Figures 8 and 9 that the large field magnitude causes a sharp drop in density and temperature close to the plasma grid. A drop in potential is also seen from Figure 10 but it is much smaller. In all three cases it is evident that a higher RF power increases the value at the antenna end as well as that at the grid.

The code is currently capable of modelling the SNIF negative ion current (H^- ions) data and the electron temperature data at the optical fibre line of sight. The model was run at a variety of different RF powers and gas flows in order to gather an appropriate range of results to compare with SNIF data. The bias insert plate voltage has not been modelled as it is currently out of the scope of this model, due to the fact that the transport equations [31] follow a classical approach and in the region 2mm from the plasma grid and the bias insert, this theory no longer applies and requires further modelling, which will be done following the work of Haas and Holmes [12]. Therefore only data taken with a bias voltage of 0V has been used for the comparison. The negative ion current results are in good agreement, as shown in Figure 11 below. In this case the measured beam current from Figure 2 has been corrected using an esimate of the stripping losses which for this gas flow rate is ~28% based on a calculation of the accelerator conductance. There is a small difference between the model and the estimated beam current at the highest RF power. Measurements at higher power and different source filling pressure would be required to undertsand if this is a feature of the model or a problem ith the beam current measurement.

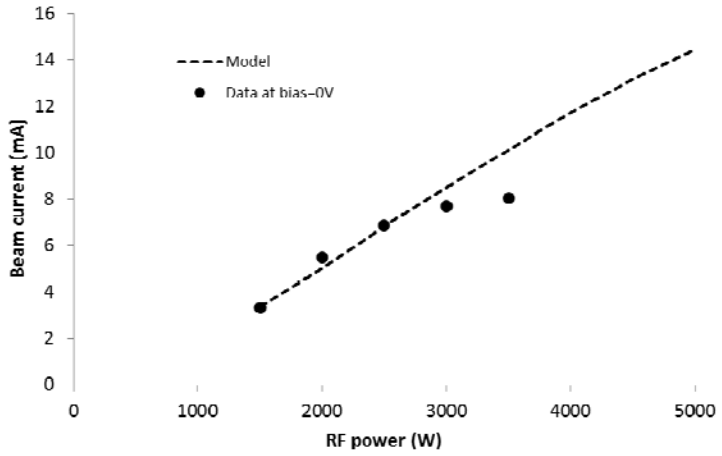

Figure 11 SNIF extracted beam current against RF power data and model output at 10sccm gas flow

The acceptance angle of the optical fibre has been accounted for in the model by taking an average of the temperature over the field of view of the lens around the centre of the fibre which is at 208.5mm along the source axis, as illustrated in Figure 9. The very rapid variation of T_e and plasma density close to the grid arising from the high magnetic field here does cause experimental problems as a minor shift in position leads to large changes in these variables. The results for T_e, using this averaging, with RF power are shown in Figure 12 with the SNIF data obtained from the coronal method as previously described in section 3.2.

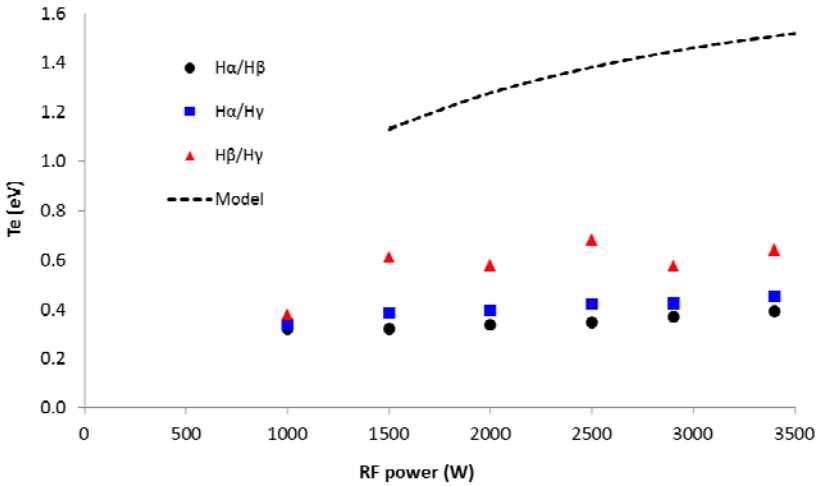

Figure 12 The electron temperature from SNIF estimated using the coronal method as a function of RF power and model output at 10sccm gas flow

Figure 12 shows that there is a discrepancy between the model output and the data, despite using the averaging method described above. This could be explained by small errors in the positioning of the line of sight and the measurement of the magnetic field since the plasma parameters are

changing rapidly in this region as shown in Figures 8,9 and 10. The coronal model is valid at plasma densities $\leq 10^{17}m^{-3}$ [25,26,27]. Since the source model predicts the density to be slightly above$10^{17}m^{-3}$ in the region of the optical fibre line of sight it could be that the coronal model is not quite valid for these conditions in the SNIF ion source. In order to verify the data it will be compared to the T_e output from a collisional radiative model and an accurate Langmuir probe measurement will also be required, to measure both T_e and n_e. If the model output and the data still disagree at this point then the model may need revising. Figure 12 also shows a difference between the experimental results for the different line ratios, in particular the H_β/H_γ ratio, due to the sensitivity and intensity of the lines as discussed in Section 2.2.

4. System studies of negative ion beamlines for future machines

The development of tokamak designs for fusion power plants generally assumes that steady state operation will be desirable for which a source of non-inductive current drive is essential. NBI is one possible current drive solution and the first system study of an NBI system for a machine beyond ITER was undertaken for an early design of the EU DEMO and concentrated on the consequences of differing geometry options for the sources and transmission into the plasma to maximise the current drive efficiency, γ [37]. It is well known [38] that economic considerations dictate the performance of the Heating & Current Drive systems and that System Code studies adopt a limiting figure of merit limiting figure of merit, F, defined as:

$$F = \gamma\varepsilon \geq 0.25 \qquad (11)$$

where ε is the electrical efficiency of HCD system, i.e. the ratio of injected power to total electrical power drawn by the system. Maximising the electrical efficiency has become the dominant theme for the development of HCD systems beyond ITER and a Neutral Beam system model was created to identify the aspects of performance that yielded the greatest benefit [21,22]. This has since been improved to include a more flexible treatment of the stripped electrons and a plasma neutraliser option. The model is based on the ITER 1MeV beamline but with additional flexibility in choice of beam current and energy, source extraction area, neutraliser model and with energy recovery systems; details are given in Table 1.

TABLE 1. Parameters for system efficiency calculation.

Ion source and beam	**Efficiencies and transmission**	**Neutralisation and energy recovery**
Energy (MeV) 1.0 – 1.5	DC efficiency 0.9	**Gas neutraliser**
D⁻ current (A) 59.1	RF efficiency 0.9	Neutralisation efficiency 0.58
Electron/D⁻ ratio 1	Stripping: No laser/laser 0.29/0.24	**Plasma neutraliser**
Electron extraction voltage (kV) 10	Stripped electron fraction 50% collected	Neutralisation efficiency 0.80
Filter field voltage (V) 5	at 200kV	**Photo-detachment**
Filter field current (A) 6000	Laser efficiency 0.25	Neutralisation efficiency 0.58-0.95
RF power (kW) 800	Incidentals (MW):	**Energy recovery**
Electron suppression voltage (V) 15	Gas neutraliser 6	Negative Ion Recovery energy (kV) 25
Electron suppression current (A) 166	Plasma neutraliser 5	Recovery fraction 0.8
Core divergence (mrad) 3-7	Photoneutraliser 4.4	Positive Ion Recovery energy (kV) 200kV
Halo divergence (mrad) 15		Conversion efficiency for positive ions 0.9

4.1 Calculation of Electrical Efficiency

The power drawn by the accelerator is determined by the specified beam extraction area, current density, co-extracted electron current and the beam energy. An electron suppression system and filter field generated by passing a current in the plasma grid are also included in the calculation. The co-extracted electron current is assumed to be deflected onto a collector grid at 10keV energy (i.e. they are not accelerated to full energy). All these dc power supplies are included in the high

voltage deck power calculation and in the wall plug load via the HV transformer efficiency. The RF power to the ion source is fed via a separate transformer and is not part of the HV deck calculation.

The gas and the passive plasma neutralizer [20] have no direct power requirement but this is not the case for the photoneutralizer. In the case of the photoneutralizer the power to the laser is given in [19]:

$$P_L = \frac{hc}{\lambda}\frac{ln(1-\eta)}{\sigma}\left(\frac{2eV_b}{m_b}\right)^{0.5}\frac{w}{G}\frac{N_w}{\eta_L} \qquad (12)$$

where λ=1064nm is the laser wavelength, σ=3.38x10^{-21} m^2 the photodetachment cross section and G=500 the cavity gain, η is the neutralization efficiency, N_w the number of laser cavities of width w and η_L is the laser power efficiency (set at 25%).

The energy recovery systems are based on the circuit shown in [21] for a conventional configuration with the injector at high voltage. Recovery of both negative and postive residual ion beams are included but the latter is connected by a converter to the HV supply [21,22]. The miscellaneous power requirement for items such as cryogenic plant, pumping, heat rejection, etc is treated as a constant with some allowance for the reduced cryogenic and pumping requirements for the photoneutraliser (Table 1).

There are three loss mechanisms acting on the beam: (i) electron loss or stripping of the negative ion in the accelerator, (ii) direct interception of the beam with beamline components such as the neutralizer and residual ion dump (if included) and (iii) re-ionization of the neutral beam downstream of the neutraliser.

The choice of neutralizer technology affects other aspects of the beamline operation. For example, the photoneutraliser introduces no gas target into the beamline, so the re-ionization and stripping losses are reduced. The size and number of injectors also influences the background gas load and in particular the re-ionization losses which have been shown to scale with the square of the injector number [37]. These effects are included in the code by a combination of scaling and logical operator.

The negative ion beam is subjected to stripping reactions as it passes through the accelerator and the beam loss is scaled from the 29% estimate for ITER [39] by extraction area, A_{ext}, to reflect the influence of the gas flow from the source. The model allows a specified fraction of stripped electrons to be collected at a specified energy to accommodate changes to accelerator pumping. A further reduction of 20% is applied if the photoneutraliser option is selected to accommodate the reduced gas pressure in the accelerator.

The direct interception loss, T, is a function of the beam core and halo divergences and has been parameterised from calculations of the ITER beamline using the BTR code [40] to be the functions:

with halo $\quad T = 0.0102\theta^2 - 0.0496\theta + 0.0711 \quad 3 \le \theta \le 7 mrad$

(13)

without halo
$$T = 0.0122\theta^2 - 0.0708\theta + 0.1029 \quad \theta > 3mrad$$
$$T = 0 \quad \theta = 3mrad$$

The re-ionization loss, R, is derived from those calculated for the ITER beamline (under normal plasma conditions i.e. excluding experimental high density plasma scenarios) by scaling for the re-ionization cross section, the beamline length, L, and the extraction area. A further reduction of 50% is made for the photoneutraliser option to reflect the reduced gas load in the beamline.

The total number of injectors, N_{inj}, is included as each injector contributes to the background gas pressure responsible for re-ionization losses.

The electrical efficiency is simply the ratio of the power transmitted to the plasma to the power drawn by the beam system including all power sources.The current drawn by the main HV supply is:

$$I_{HV} = I_{ext}\left(1 - \kappa_{strip} f_{strip} - f_{rec}^{-} F^{-}\right) \tag{14}$$

where I_{ext} is the extracted ion current, κ_{strip} is the fraction of the stripped electron current, f_{strip}, that is collected on the intermediate grids at potential V_{acc} and the fraction of the residual negative ion current, F^-, collected by the recovery system, f_{rec}^{-}, is re-circulated through the main HV supply. The main HV power is:

$$P_{HV} = V_b I_{HV} + \kappa_{strip} f_{strip} I_{ext} V_{acc} \tag{15}$$

Thus the total wall plug power to the HV deck through the transformer is:

$$P_{drain} = \left(P_{HV} + P_{aux}\right)/\eta_{DC} \tag{16}$$

where P_{aux} is the total power drawn by auxiliary source systems such as the filter field. Note that the DC efficiency, η_{DC}, effectively appears as a squared term for the auxiliary supplies as it has been assumed that the conversion efficiency from the transformer output to DC is equivalent to that for the transformer itself.

The wall plug efficiency is simply obtained from the ratio of the beam power injected to the plasma to the sum of the HV deck and non-HV deck electrical power:

$$\varepsilon = \frac{P_{plas}}{P_{elec}} = \frac{I_{ext} V_b \left(1 - f_{strip}\right)\eta\left[1 - \left(T + R\right)\right]N_{inj}}{\left(P_{drain} + P_{rsys}^{-} + P_L + P_{mis} - P_{rec}^{+}\right)N_{inj}} \tag{17}$$

where η is the neutralisation efficiency. The energy recovery systems are represented by P_{rsys}^{-} the power supplied to the negative ion energy recovery system and P_{rec}^{+}, the power recovered, converted and recirculated from the positive ion system. P_{mis} is the power supplied to various miscellaneous beamline systems including cryo- and vacuum pumps. This is set at 6MW for the gas neutraliser, 5MW for the plasma neutraliser (due to the reduced gas density) and 4.4MW for the photoneutraliser. Note that the number of injectors, N_{inj}, appears to cancel but, in fact maintains an influence through the re-ionization losses. In reality this is usually quite small so the advantage of improved reliability with several smaller injectors does not translate into efficiency.

4.2 Electrical Efficiency Results

The model has been used to investigate the sensitivity of efficiency to various parameters. The greatest impact is, of course, the choice of neutralizer and the results are shown in Figure 13 for the three neutralizer types. As expected, the efficiency with a plasma neutraliser is intermediate to the gas and photoneutraliser. Typical current drive efficiency for 1MeV NBI in a DEMO plasma is between 0.4 and 0.45 depending on the plasma profile [40], so to satisfy the figure of merit condition in equation (11) requires an electrical efficiency in the range $\varepsilon \sim 0.55 - 0.6$. Raising the beam energy to 1.5MeV increases the value of γ by ~10% once limitations due to shinethrough are considered [41] thus dropping the required efficiency to $\varepsilon \sim 0.5$, a value that might be achievable with improvements to beam divergence. Given the relative simplicity of the passive plasma neutralizer in comparison to the engineering complexity of the photoneutraliser this seems to be a promising technology.

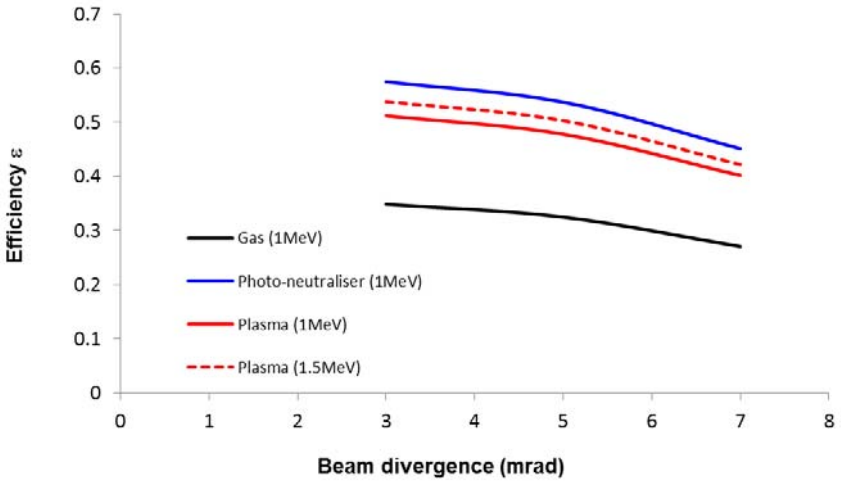

Figure 13 Electrical efficiency as a function of beam divergence for the three neutraliser options in the systems model. Gas neutraliser efficiency 58%, plasma neutraliser efficiency 80% and photo-neutraliser efficiency 90%. No energy recovery is used.

The model also allows the stripping fraction to be varied and the effect of this is shown in Figure 14, together with the impact of adding energy recovery systems. For the gas neutraliser. It is clear that a reduction in stripping losses brings significant dividend, as expected and that for the gas neutraliser the use of negative and positive ion recovery in tandem can increase the efficiency to values that satisfy the condition in equation (11). The model also shows that at 1MeV a modest reduction in stripping losses in a plasma neutraliser system coupled to recovery of the negative ion energy can reach efficiencies equivalent to the photoneutraliser.

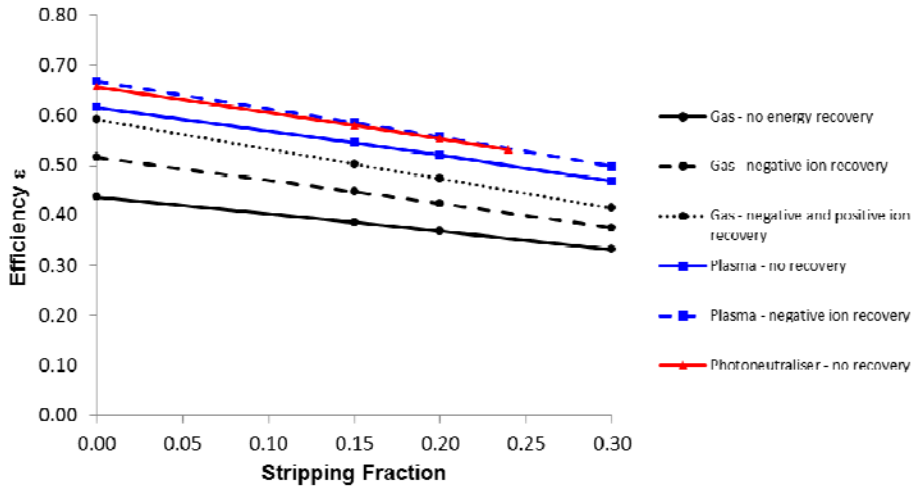

Figure 14 Effect of stripping losses and energy recovery for the three neutralisers (all at 1MeV and 5mrad divergence). Gas neutraliser efficiency 58%, plasma neutraliser efficiency 80% and photo-neutraliser efficiency 90%.

5. Conclusion and future work

The SNIF RF ion source shows a very favourable ratio of the co-extracted electron to H^- current of <1 over the range of operating parameters. This is achieved even with zero bias voltage on the insert in the plasma grid. Such performance is normally difficult in volume ion sources and the use of caesium is needed to reduce the extracted electrons to below the negative ion current. Thus SNIF represents an ideal test bed to advance the physics understanding in these sources. This has begun with the use of spectroscopy to measure the electron temperature from the Balmer line ratios. A coronal model has been used to date to obtain the electron temperature but a collisional-radiative model (CR) may be more appropriate. The spectroscopy can also be used to obtain gas temperatures and the degree of dissociation in the ion source plasma. In addition it is planned to use a Langmuir probe as an alternative technique to measure plasma temperature and density. The low electron to negative ion ratio may be associated with the relatively strong magnetic field near the extraction plane due to the filter field and the magnets used in the plasma grid to suppress the extracted electrons. The 1D fluid model of the discharge will be used to understand the role of this magnetic field on both the negative ions and co-extracted electrons providing a predictive tool to guide changes to the ion source configuration.

If neutral beam systems are to be used in future fusion machines for heating and current drive then it is essential for economic viability that the electrical efficiency of these sub-systems must be improved significantly. Relatively straightforward systems studies have provided a valuable insight into understanding what the benefits and limitations are of various technologies, e.g. photo or plasma neutralsiers and energy recovery and conversion of the residual negative and positive ions after the neutraliser. For instance it is clear that the passive (beam driven) plasma neutraliser may offer a considerable improvement over a conventional gas neutraliser. The neutralisation efficiency of the plasma neutraliser may not reach that which is potentially available from a photo-neutraliser but it would involve much less of a technological risk. Testing of the basic physics of a beam driven plasma neutraliser could be carried out on a facility such as SNIF and work is underway to understand the plasma generation from both negative and and positive ion

beams at low energy to determine the basic scaling laws and the level of plasma generation with the beams from SNIF.

Acknowledgements

This work has been carried out within the framework of the EUROfusion Consortium and has received funding from the Euratom research and training programme 2014-2018 under grant agreement No 633053 and from the RCUK Energy Programme [grant number EP/I501045]. To obtain further information on the data and models underlying this paper please contact PublicationsManager@ccfe.ac.uk. The views and opinions expressed herein do not necessarily reflect those of the European Commission.

References

[1] J. M. Wadehra and J. N. Bardsley, Phys. Rev. Lett., **41**, 1795–1798 (1978)

[2] M. Bacal and G. W. Hamilton, Phys. Rev. Lett., **42**, 1538–1540 (1979)

[3] K.N. Leung, K.W. Ehlers and M. Bacal, Lawrence Berkeley Laboratory report LBL-14292, (1982)

[4] A.J.T. Holmes Rev. Sci. Instrum. **53**, 1517-1522 (1982); http://dx.doi.org/10.1063/1.1136828

[5] A.J.T. Holmes Rev. Sci. Instrum. **53**, 1523-1526 (1982); http://dx.doi.org/10.1063/1.1136829

[6] A.J.T. Holmes and T.S. Green, 3rd Int. Symp. on Production and Neutralisation of Negative Ion Beams, Brookhaven, AIP Conf. Proc. **111** 429-437 (1983); http://dx.doi.org/10.1063/1.34369

[7] A.J.T. Holmes, G. Dammertz and T.S. Green Rev. Sci. Instrum., **56**, 1697-1702 (1985); http://dx.doi.org/10.1063/1.1138126

[8] A.J.T. Holmes and M.P.S. Nightingale, Rev. Sci. Instrum., **57**, 2402-2408, (1986); http://dx.doi.org/10.1063/1.1139085

[9] M. P. S. Nightingale, A. J. T. Holmes and J. D. Johnson, Rev.. Sci. Instr. **57**, 2396 (1986); *http://dx.doi.org/10.1063/1.1139084*

[10] R. McAdams, A.J.T. Holmes and M.P.S. Nightingale, Rev. Sci. Instrum., **59**, 895-901 (1988); http://dx.doi.org/10.1063/1.1139799

[11] R. McAdams, R. F. King, A. J. T. Holmes and G. Proudfoot, Plasma Sources Sci. & Technol., **2**, 86-92 (1993); http://dx.doi.org/10.1088/0963-0252/2/2/003

[12] F. Haas and A.J.T. Holmes, Plas. Phys. and Control. Fusion, **33**, 1197-1211 (1991); http://dx.doi.org/10.1088/0741-3335/33/10/006

[13] R. McAdams, R.F. King and A.F. Newman, Rev. Sci. Instrum., **61**, 2176-2183 (1990); http://dx.doi.org/10.1063/1.1141386

[14] R. McAdams, R.F. King and A.F. Newman, Rev. Sci. Instrum., **63**, 1777-1782, (1992); http://dx.doi.org/10.1063/1.1143337

[15] R. McAdams, A.J.T. Holmes, D.B. King and E. Surrey, Plasma Sources Sci. Technol. **20,** 035023 (2011), doi:10.1088/0963-0252/20/3/035023

[16] E. Surrey, Nucl. Fusion **46** S360–S368 (2006), doi:10.1088/0029-5515/46/6/S18

[17] E. Surrey, A.J.T. Holmes, D.B. King and R. McAdams, J Fusion Energy **29**, 486–498 (2010); doi: 10.1007/s10894-010-9311-1

[18] E. Surrey, Proceedings of 11th International Symposium on the Production and Neutralization of Negative Ions and Beams, AIP Conf. Proc. **925,** 278-289 (2013); http://dx.doi.org/10.1063/1.2773666

[19] M. Kovari and B. Crowley, Fusion Engineering and Design **85,** 745–751 (2010); doi:10.1016/j.fusengdes.2010.04.055

[20] E. Surrey and A.J. T. Holmes, Proceedings of the Third International Symposium on Negative Ions, Beams and Sources (NIBS 2012), AIP Conf. Proc. **1515** 532-540 (2013); http://dx.doi.org/10.1063/1.4792825

[21] R. McAdams, A. J. T. Holmes, M. Porton, A. Benn, E. Surrey and T.T.C. Jones, Proceedings of the Third International Symposium on Negative Ions, Beams and Sources (NIBS 2012), AIP Conf. Proc. **1515** 559-568 (2013); http://dx.doi.org/10.1063/1.4792828

[22] R. McAdams, Rev. Sci. Instr. **85**, 02B319 (2014); http://dx.doi.org/10.1063/1.4852299

[23] J. Zacks et al., Proceedings of the First International Symposium on Negative Ions, Beams and Sources (NIBS 2012), AIP Conf. Proc. **1515** 569 (2013); http://dx.doi.org/10.1063/1.4792829

[24] E. Speth et al., Nucl. Fusion **46** (2006) S220–S238; doi:10.1088/0029-5515/46/6/S03

[25] U. Fantz, Plasma Sources Sci. Technol. **15**, S137-147 (2006); http://dx.doi.org/10.1088/0963-0252/15/4/S01

[26] R.F. Boivin, J. L. Kline and E. E. Scime, Phys. Plasmas **8,** 5303-5314 (2001); http://dx.doi.org/10.1063/1.1418020

[27] J. Komppula and O Tarvainen, Plasma Sources Sci. Technol. **24,** 045008 (2015); doi:10.1088/0963-0252/24/4/045008

[28] Hydkin database, available at http://www.hydkin.de/

[29] A.J.T. Holmes Plasma Sources Sci. Technol. **5** 453–73 (1996) ; http://dx.doi.org/10.1088/0963-0252/5/3/014

[30] E. Surrey and A.J.T. Holmes Plasma Sources Sci. Technol. **24** 015035 (2015) ; http://dx.doi.org/10.1088/0963-0252/24/1/015035

[31] E. Surrey and A.J.T. Holmes Plasma Sources Sci. Technol. **24** 015036 (2015) ; http://dx.doi.org/10.1088/0963-0252/24/1/015036

[32] E.M. Epperlein and M.G. Haines Phys. Fluids **29** 1029-1041 (1986) ; http://dx.doi.org/10.1063/1.865901

[33] J.T. Gudmundsson and M.A. Lieberman Plasma Sources Sci. Technol. **6** 540–550 (1997) ; http://dx.doi.org/10.1088/0963-0252/6/4/012

[34] A.T. Hjartarson, E.G. Thorsteinsson and J.T. Gudmundsson Plasma. Sources Sci. Technol. **19**, 065008 (2010); http://dx.doi.org/10.1088/0963-0252/19/6/065008

[35] C.F. Chan, Lawrence Berkeley Laboratory Report LBID-632 (1983)

[36] J.R. Hiskes and A.M. Karo, J Appl. Phys. **67**, 6621-6632 (1990); http://dx.doi.org/10.1063/1.345095

[37] E. Surrey, A. Benn,I. Jenkins,M. Porton,W. Timmis,A. Turner, Fusion Engineering and Design **87** 373-383 (2012) doi:10.1016/j.fusengdes.2012.03.028

[38] E. Surrey1, C. Challis1, I. Jenkins1, and K. David1 Proc 24th IAEA Fusion Energy Conference, San Diego, USA 8-13 October 2012 FTP/P1/26 http://www-naweb.iaea.org/napc/physics/FEC/FEC2012/html/proceedings.pdf

[39] E. Sartori, et al., Rev. Sci. Instrum. **85**, 02B308 (2014); http://dx.doi.org/10.1063/1.4827677

[40] E. Dlougach et.al. *http://www.btr.org.ru*

[41] I. Jenkins, C.D. Challis, D.L. Keeling and E Surrey, Fusion Engineering and Design **106** 9-16 (2016) doi:10.1016/j.fusengdes.2016.02.077